EURASIP Journal on Wireless Communications and Networking

RESEARCH Open Access

Underwater acoustic FBMC communication with multiple mode index modulation

Ziqian Li[1], Biao Wang[1], Tao Fang[1*], Yunan Zhu[2] and Haotian Lyu[3]

*Correspondence:
fangtao@just.edu.cn

[1] Ocean College, Jiangsu University of Science and Technology, Zhenjiang 212003, China
[2] Institute of Acoustics, Chinese Academy of Science, Beijing 100190, China
[3] School of Engineering, Tokai University, Hiratsuka, Japan

Abstract

In underwater acoustic communication (UWA), there is a significant presence of multipath and Doppler spread. The integration of orthogonal frequency division multiplexing (OFDM) with index modulation (IM), utilizing subcarrier index modulation to enhance system performance underwater, has garnered considerable interest from researchers. Multiple mode modulation can enhance utilization by transmitting symbols of different modes on different subcarriers. Inspired by the concepts of index modulation and multiple mode modulation, this paper proposes a method that combines multiple mode indexing with the filter bank multicarrier system (MM-FBMC-IM), enabling the transmission of different modulation orders on each subcarrier to increase system flexibility. Simulations demonstrate that under the same spectral efficiency, multiple mode indexing FBMC offers superior bit error rate (BER) performance compared to conventional FBMC and index modulation FBMC.

Keywords: FBMC, Index modulation, Multiple mode, Euclidean distance, Underwater acoustic communication

1 Introduction

Underwater acoustic communication has become a hot topic in recent years. OFDM technology, known for its high spectral efficiency, multi-path fading resistance, and flexibility, is widely used [1, 2]. IM has already developed quite maturely within OFDM systems. The basic idea of index modulation is to transmit additional information through the indices of signal elements such as frequency, time, and space. The combination of index technology with OFDM systems, known as orthogonal frequency division multiplexing with index modulation (OFDM-IM), is the mainstream development of index modulation today. For example, noncoherent OFDM-IM is considered, where information bits are transmitted solely through the indices of active subcarriers [3, 4]. Someone proposed the application of OFDM-IM for underwater acoustic (UWA) channels, introducing a hybrid scheme to enhance spectral efficiency, and also proposed a new self-cancellation method for ICI in OFDM-IM [5]. To reduce the PAPR of OFDM, a new scheme for UWA communication was proposed—pre-coded index modulation orthogonal frequency division multiplexing spread spectrum (IM-OFDM-SS) [6].

However, since the inactive subcarriers in OFDM-IM cannot modulate information and the active subcarriers only adopt the same modulation mode, the spectral efficiency of OFDM-IM is not high. To improve the spectral efficiency of OFDM-IM, a dual-mode OFDM technology (DM-OFDM) has been proposed, which combines with index modulation to enhance the throughput of traditional OFDM based on index modulation [7]. To increase the system's flexibility, where the number of subcarriers modulated by the same constellation pattern in each subblock is variable, dual-mode indexing has also been proposed [8], further improving the system's spectral efficiency. A modulation scheme for the multiple mode orthogonal frequency division multiplexing with index modulation (MM-OFDM-IM) system has been proposed [9]. Scholars have proposed the coordinate interleaving (CI-) MM-OFDM-IM and linear constellation precoding (LCP-) MM-OFDM-IM-IQ schemes, both of which achieve second-order diversity without losing spectral efficiency [10].

Further advancements have been proposed a composite multiple-mode orthogonal frequency division multiplexing with index modulation (C-MM-OFDM-IM) and two enhancement schemes, named Generalized C-MM-OFDM-IM (II) and C-MM-OFDM with In-phase/Quadrature IM (II), respectively. The former considers a joint approach involving all SAPs, EAPs, CAPs, and modulation symbols, while the latter extends the implementation of indexing to the in-phase and quadrature constellation domains [11]. In the OFDM-IM system, someone proposed the capability of signal detection using deep learning. They introduced a scheme based on Y-shaped networks with fully connected layers (Y-FC) and bidirectional long short-term memory units (Y-BLSTM) to further optimize data reception [12]. In the orthogonal time frequency space (OTFS) system, there has also been an integration of indexing, such as the proposal of a spatial multiplexing aided orthogonal time frequency space index modulation (OTFS-IM). This approach combines the advantages of OTFS-IM and vertical bell laboratories layered space-time (VBLAST) technology [13]. Scholars have also proposed a new transmission scheme, termed orthogonal time frequency space with dual-mode index modulation (OTFS-DM-IM), aimed at balancing transmission reliability and spectral efficiency [14]. In UWA channels, an OTFS-IM underwater communication system based on Hamming distance optimization was proposed to mitigate the effects of dispersion on underwater communications [15]. Although the combination of index modulation and FBMC technology is still rare, it is still worth referring to in underwater acoustic communications. Someone proposed a doppler frequency shift estimation for the FBMC/OQAM system in underwater acoustic channels based on frame boundary detection and deep learning. The proposed CNN-based doppler scale estimator and stacked autoencoder doppler scale estimator have better performance in UWA channels [16]. Due to the severe interference in underwater acoustic channels, a Lattice Reduction-Aided Sphere Decoder (LRA-SD) has been proposed. This receiver has better computational efficiency compared to traditional receivers [17]. Someone analyzed the residual doppler effect in multipath underwater acoustic channels within FBMC/OQAM systems. Under UWA channels, in the presence of residual doppler effects, FBMC exhibits better bit error rate performance compared to OFDM based on CP [18].In the realm of deep learning, an effective method based on complex valued neural networks (CVNN) has been proposed for accurate channel estimation of FBMC/OQAM signals with lower computational

complexity and pilot overhead [19]. Scholars have proposed a FBMC system for underwater acoustic communication based on convolutional neural networks (CNN). Unlike traditional FBMC receivers, which detect transmitted symbols only after explicit channel estimation and equalization, this system utilizes a pre-trained CNN model as the receiver to directly recover transmitted symbols, thereby avoiding inherent imaginary part interference [20]. In [21], the multimode index technique is combined with MIMO-OFDM technology, leveraging the advantages of both techniques. In [22], a high-dimensional mapping scheme is proposed to reduce multimode interference. In a recent article, a new FBMC communication scheme was proposed, which carries additional information by mapping the real and imaginary parts of the symbol to time-frequency points separately [23].

The paper compares the performance of MM-FBMC-IM with conventional FBMC and index modulation FBMC in underwater acoustic channels.

This paper primarily investigates the FBMC in underwater acoustic channels. By integrating FBMC with multiple mode indexing, we propose MM-FBMC-IM, which enhances the system's spectral efficiency. Additionally, the multiple mode indexing in this paper allows for the selection of subcarriers to transmit symbols from different modulation order constellation diagrams, thereby increasing the system's flexibility.

The main structure of this paper is as follows: In Sect. 2, we introduce the experimental environment and the method models used in the experiment. In Sect. 3, the derivation of the system's transmission and reception is introduced, along with an analysis of spectral efficiency and the detection methods used in the experiment. In Sect. 4, we conduct simulation experiments and demonstrate the advantages of the proposed methods through comparative experiments. In Sect. 5, result analysis and discussion are conducted.

The main contributions of this paper are as follows:

- We propose the MM-FBMC-IM system that combines multi-mode index modulation with the FBMC system by transmitting different modes on each subcarrier. Under the same conditions, this can improve system throughput.
- Different order symbols of different modes can be transmitted on each subcarrier, enhancing the system's flexibility.
- By applying the MM-FBMC-IM system to actual underwater acoustic channels, we find that this system can achieve better BER performance compared to traditional systems at the same spectral efficiency.

2 Methods/experimental

In this section, we mainly introduce the transmitter of the system described in this paper, as well as the methods of index mapping and symbol mapping.

2.1 MM-FBMC-IM system

The MM-FBMC-IM system is built upon the framework of the classical FBMC system, as shown in Fig. 1. The total number of bits transmitted is denoted as m, Firstly, we divide all N subcarriers into G groups, from which we can obtain the number of subcarriers per group as $n = N/G$. In MM-FBMC-IM, each group of subcarriers is comprised

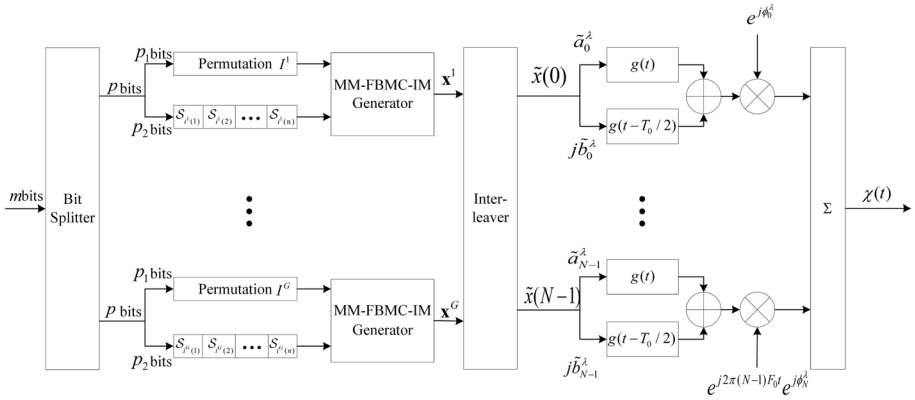

Fig. 1 MM-FBMC-IM system block diagram

Table 1 Mapping table for $n = 3, p_1 = 2, c = 2^{p_1} = 4$ configuration

Bits	Index combination I^{β}	Signal constellation
[0 0]	{1,2,3}	$\{S_1, S_2, S_3\}$
[0 1]	{1,3,2}	$\{S_1, S_3, S_2\}$
[1 0]	{2,1,3}	$\{S_2, S_1, S_3\}$
[1 1]	{3,2,1}	$\{S_3, S_2, S_1\}$
Invalid	{2,3,1}	$\{S_2, S_3, S_1\}$
Invalid	{3,1,2}	$\{S_3, S_1, S_2\}$

of different mode combinations. The processing method for the data in each group is the same. For ease of understanding, we will only consider one block β, $\beta \in 1, \cdots, G$. In the diagram, the index selector uses p_1 bits, also known as index bits, to control the arrangement of signal modes for n subcarriers, while the other p_2 bits, also referred to as symbol bits, control the constellation mapping of the modes. Therefore, the total number of bits can be represented as $p = p_1 + p_2$.

This paper primarily employs phase shift keying (PSK) modulation. For PSK modulation, each group is composed of n subcarriers, thus utilizing n different modes of PSK signals. Moreover, the order of these various modes of signals can differ, denoted as M. The constellation of different modes of M-order PSK signals is obtained by rotating their initial M-order PSK constellation by an angle of $2\pi(L-1)/nM$, where $L = 1, \cdots, n$.

2.2 Index bit mapping method

Since there can be at most n permutation results in the system, p_1 can carry at most $\lfloor \log_2(n!) \rfloor$ bits, i.e., $p_1 = \lfloor \log_2(n!) \rfloor$. The permutations I^{β} that can be generated by the index bits p_1 can be realized using the following two methods:

a) Lookup table method: The lookup table method is quite straightforward to understand. We only need to first generate 2^{p_1} constellation combination methods and their corresponding bits. For example, Table 1 is for $n = 3$, while $p_1 = \lfloor \log_2(3!) \rfloor = 2, c = 2^{p_1} = 4$, and c is the total number of permutation methods. Among them, since there are six total permutation methods, and two bits can

represent at most four states, there exist two unused (invalid) combinations in the total permutation methods. When n is small, this method can indeed be convenient, but as n becomes larger, this method will become very complex.

b) Combinatorial Number Method: The core principle of this method is that each natural number can be mapped to a permutation result of a set. Moreover, it is possible to find a unique sequence $J = \{ a_n, \cdots, a_1 \}, a_1, \cdots, a_n \in \{ 1, \cdots, n \}$ that satisfies Z.

On this basis, remove

$$Z = (a_n - 1) * (n-1)! + \cdots + (a_2 - 1) * (1)! + (a_1 - 1) * 0! \tag{1}$$

On this basis, remove certain combinations to ensure that $c = 2^{p_1} = 4$. Similarly, the combinatorial method [24] also discards two index combination methods in this case, where $p_1 = 2$.

2.3 Symbol mapping

The block diagram for different modes of the same order is as shown in Fig. 2, signals in different modes are obtained by rotating them by different angles, for example, starting from angle 0, n types of M-PSK modes can be easily obtained by rotating the original M-PSK (angle 0) constellation by an angle of and $2\pi(L-1)/nM$, where $L = 1, ..., n$.

Selecting the sub-constellation modes used on each subcarrier is a critical issue for the system to obtain optimal BER performance. It is essential to maximize both the minimum intra-mode distance (MIAD) and the minimum inter-mode distance (MIRD).

As shown earlier, each subblock carries different modes on n subcarriers, meaning these n subcarriers correspond one-to-one with the constellation of n different

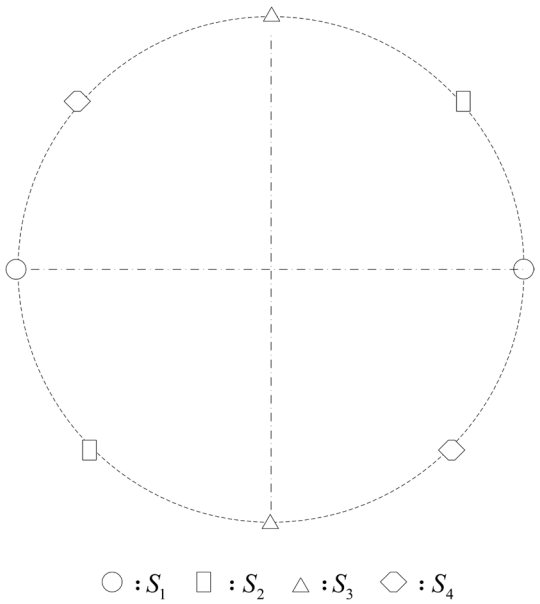

Fig. 2 Constellation diagrams of BPSK signals for four different modes with $n = 4$

modes of M-order PSK signals. Therefore, the combination of these different modes is a result of a permutation, which implies that p_1 bits determine the permutation of set $\Omega = 1, \cdots, n$, resulting in one permutation outcome of set $\Omega = 1, \cdots, n$:

$$\mathrm{I}^{\beta} = \left\{ i^{\beta}(1), \cdots, i^{\beta}(n) \right\} \tag{2}$$

wherein, $i^{\beta}(\alpha) \in \{1, \cdots, n\}, \alpha \in \{1, \cdots, n\}$. In FBMC-IM, I^{β} denotes the positions of the activated subcarriers, while the remaining subcarriers remain silent and do not transmit symbols. In the MM-FBMC-IM system, I^{β} represents the full permutation of all transmission modes, and all subcarriers will be activated. Therefore, the signal constellation of different modes used by n subcarriers can be represented as:

$$\left\{ \mathcal{S}_{i^{\beta}(1)}, \cdots, \mathcal{S}_{i^{\beta}(n)} \right\} \tag{3}$$

wherein, $\mathcal{S}_{i^{\beta}(\alpha)}$ represents the signal constellation used by the α^{th} subcarrier, and the average power of $\{\mathcal{S}_1, \cdots, \mathcal{S}_n\}$ has been normalized to unit power.

The symbol bits are set to $p_2 = n\log_2(M)$, and the output of the constellation mapper is denoted as $\left[s^{\beta}(1), \cdots, s^{\beta}(n) \right]^T, s^{\beta}(n) \in \mathcal{S}_{i^{\beta}(\alpha)}$.

Next, we introduce the transmission methods for different modes and different orders. Similar to the aforementioned multiple mode modulation constellation diagram, the difference is that while adjusting the modes by changing the rotation angles, we also modify the order of the modes, making the system more flexible and controllable. Firstly, assume the number of signal constellations for an M_k-order is n_k, then it needs to satisfy $\sum_{k=1}^{K} n_k = n, M_1 > M_2 > \cdots > M_k$. To facilitate understanding, let's provide an example

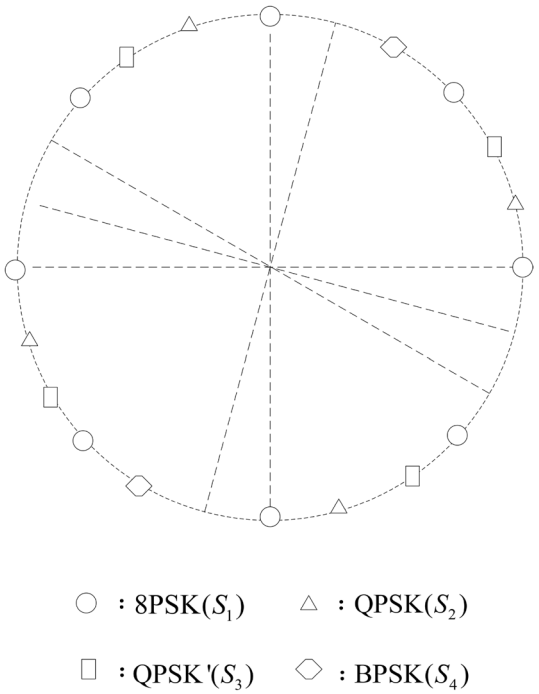

Fig. 3 Constellation diagrams of signals for four different modes with four different orders, where $n = 4$

with $(M_1(n_1), M_2(n_2), M_3(n_3)) = (8(1), 4(2), 2(1))$, as shown in Fig. 3. This figure depicts a constellation diagram that includes one 8PSK, two types of QPSK, and one BPSK signal. Similar to the approach with different modes of the same order, it also adheres to the principle of maximizing both the MIAD and the MIRD.

In this case, the symbol bits $p_2 = \sum_{k=1}^{K} n_k \log_2(M_k)$.

Although the symbol bits p_2 differ between the two multiple mode methods, the transmission process for both multiple mode methods is the same. After modulation through MM-FBMC-IM, the output data for each group is as follows:

$$\mathbf{x}^{\beta} = \left[x^{\beta}(1), \cdots, x^{\beta}(n)\right]^T \tag{4}$$

where $x^{\beta}(\alpha) \in s^{\beta}(\alpha), \alpha = 1, \cdots, n$, and $\mathbf{x}^{\beta}$ represents the data after passing through the MM-FBMC-IM generator.

3 Derivation of sending and receiving signals

After generating all MM-FBMC-IM data groups through the generator, the data will pass through a $G \times n$-dimensional interleaver, resulting in the interleaved data being:

$$\tilde{\mathbf{x}}^{\lambda} = \left[\tilde{x}^{\lambda}(0), \tilde{x}^{\lambda}(1), \cdots, \tilde{x}^{\lambda}(N-1)\right]^T \tag{5}$$

$$= [x^1(1), x^2(1), \cdots, x^G(1), \cdots, x^1(n), x^2(n), \cdots, x^G(n)]^T \tag{6}$$

where λ represents the number of symbols to be transmitted by MM-FBMC-IM.

The interleaved data, after passing through the transmitter; filter modulation output, ultimately yields the transmitted signal of MM-FBMC-IM as:

$$\chi(t) = \sum_{l=0}^{N-1} \sum_{\lambda=0}^{+\infty} e^{j2\pi l F_0 t} e^{jd\phi_l^{\lambda}} \left(\tilde{a}_l^{\lambda} g(t - \lambda T_0) + j\tilde{b}_l^{\lambda} g(t - \lambda T_0 - \frac{T_0}{2}) \right) \tag{7}$$

where l represents the subcarrier index, F_0 and T_0, respectively represent the subcarrier spacing and symbol period, with $F_0 = 1/T_0$. $g(t)$ is the prototype filter function, and $\Phi_{l,k} = l\pi/2$ is the added rotational phase. $\tilde{a}_l^{\lambda}$ and $\tilde{b}_l^{\lambda}$ represent the real or imaginary part of the symbol, respectively. Since, it is multiple mode indexing, the values of $\tilde{a}_l^{\lambda}$ and $\tilde{b}_l^{\lambda}$ might be one of the modes in $s^{\beta}(\alpha)$.

Assuming that the current channel state information is perfectly estimated, after channel equalization and deinterleaving, the receiver's MM-FBMC-IM demultiplexer divides the received data into G groups. The received signal of the β^{th} subblock, $\mathbf{y}_f^{\beta}$ can be represented as:

$$\mathbf{y}^{\beta} = \left[y^{\beta}(1), \cdots, y^{\beta}(n)\right]^T = \mathbf{X}^{\beta}\mathbf{h}^{\beta} + \mathbf{w}^{\beta} \tag{8}$$

where,$\mathbf{X}^{\beta} = \mathrm{diag}(\mathbf{s}^{\beta}), \mathbf{h}^{\beta} = \left[\, h^{\beta}(1) \ \cdots \ h^{\beta}(n) \,\right]^T, \mathbf{w}^{\beta} = \left[\, w^{\beta}(1) \ \cdots \ w^{\beta}(n) \,\right]^T$. $\mathbf{w}^{\beta}$ is the frequency domain noise, and $\mathbf{h}^{\beta}$ is the vector of channel frequency domain fading

coefficients.,$\mathbf{w}^{\beta}$ and $\mathbf{h}^{\beta}$ follow $\mathcal{CN}(\mathbf{0}, N_0\mathbf{I_n})$ and $\mathcal{CN}(0, \mathbf{I_n})$ distributions, respectively. N_0 is the noise variance in the frequency domain.

This article primarily analyzes multiple mode index modulation, and we only briefly introduce the detection algorithm used for demodulation. We employed the maximum likelihood (ML) detection: At the receiver, by searching through all possible scenarios of subblocks to minimize the value of the formula below, the transmitted symbols $\hat{\mathbf{s}}^{\beta}$ and the index permutations $\hat{\mathbf{I}}^{\beta}$ for each subblock are estimated:

$$(\hat{\mathbf{s}}^{\beta}, \hat{\mathbf{I}}^{\beta}) = \arg\min_{s^{\beta}, 1^{\beta}} \mathbf{y}^{\beta} - \mathbf{X}^{\beta}\mathbf{h}^{\beta 2} \tag{9}$$

In this context, where $\hat{s}^{\beta} = \left[\hat{s}^{\beta}(1), \cdots, \hat{s}^{\beta}(n)\right]^{T}$,$\hat{\mathrm{I}}^{\beta} = \left\{\hat{i}^{\beta}(1), \cdots, \hat{i}^{\beta}(n)\right\}$. For each subblock, there are M^n different realizations of n symbols of order M, and there are p_1 different realizations of the index permutation $\hat{\mathbf{I}}^{\beta}$. Therefore, the complexity of the ML detection algorithm is $\mathcal{O}\left(2^{\lfloor \log_2(n!) \rfloor} M^n\right)$. The complexity of the traditional FBMC-IM system's ML detection algorithm is $\mathcal{O}\left(2^{\lfloor \log_2 C(n,k) \rfloor} M^k\right)$, $C(n,k)$ represents the number of combinations, and k indicates the number of active subcarriers. and it can be observed that its complexity has increased. Therefore, we consider using a low-complexity ML detection algorithm applicable to MM-FBMC-IM:

First, we will use an $n \times n$ matrix P^{β} where the decision symbol for the x-th subcarrier under the y-th signal constellation mode is represented by $\mathrm{P}^{\beta}(x, y)$.It is represented by the following equation:

$$\mathrm{P}^{\beta}(x, y) = \arg\min_{s \in S_y} \left| y^{\beta}(x) - s^{*} h^{\beta}(x) \right|^2, x, y \in \{1, \cdots, n\} \tag{10}$$

Then, an $n \times n$ matrix $\mathrm{G}^{\beta}(x, y)$ is used to represent the metric corresponding to each hard decision symbol, with x and y similarly representing the respective element indices. It is represented by the following equation:

$$\mathrm{G}^{\beta}(x, y) = \left| y^{\beta}(x) - \mathrm{P}^{\beta}(x, y)^{*} h^{\beta}(x) \right|^2 \tag{11}$$

The algorithm implements the subblock detection process through a detection tree. Each layer's detection path consists of the corresponding signal constellation mode index and the metric value of the hard decision symbol. The cumulative metric value is calculated by retaining the smallest η valid paths at each layer. Finally, in the last layer, the path with the smallest cumulative metric value is selected as the output, resulting in the estimation of the subblock's index permutation and the transmitted symbol vector.

The final computational complexity of this algorithm is $\mathcal{O}(Mn^2 + n)$. When the value of n is large, the complexity is significantly reduced.

The analysis of spectral efficiency. We will explain from two different multiple mode modulation scenarios.

For different modes with the same order in MM-FBMC-IM, the spectral efficiency can be expressed by the following equation:

Table 2 Simulation parameters

Parameter/metric	Value/condition
Subcarrier number	512
Baseband bandwidth	6400 Hz
Sampling rate	128,000 Hz
Modulation	Multiple PSK
Convolutional coding rate	1/2
Generator polynomials	[5, 7] (Octal)
Prototype filter	PHYDYAS, Overlap Factor = 4

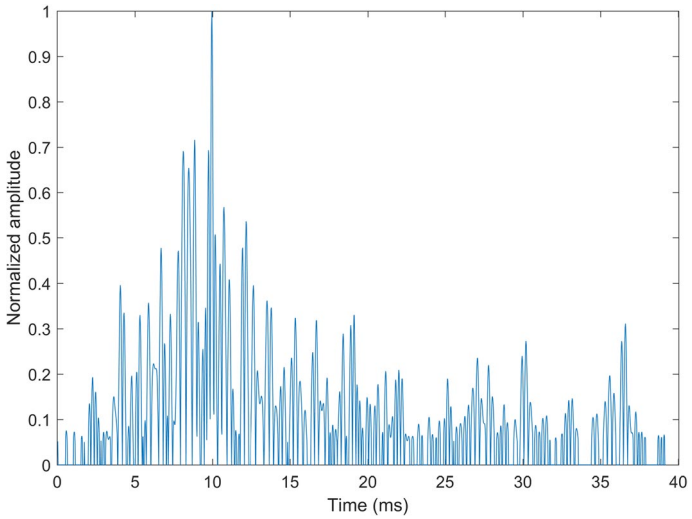

Fig. 4 Channel impulse response measured at 5 km in the Bohai Sea

$$\eta = \frac{m}{N} = \frac{p}{n} = \frac{\log_2(n!) + n\log_2(M)}{n} [\text{bps/Hz}] \tag{12}$$

We can see that the spectral efficiency at this time is determined by the number of subcarriers and the order, and it is relatively fixed without many options. The spectral efficiency of MM-FBMC-IM for different modes and orders can be expressed as:

$$\eta = \frac{m}{N} = \frac{p}{n} = \frac{\log_2(n!) + \sum_{k=1}^{K} n_k \log_2(M_k)}{n} [\text{bps/Hz}] \tag{13}$$

At this point, although the spectral efficiency is still determined by the number of subcarriers and the order, we can choose different order modes to transmit on each subcarrier, making the system flexible and controllable.

4 Simulation results

In this section, we will compare traditional FBMC, FBMC-IM, and MM-FBMC-IM to analyze their performances. The comparison is conducted under the principle of maintaining the same data rate to highlight the advantages of MM-FBMC-IM.

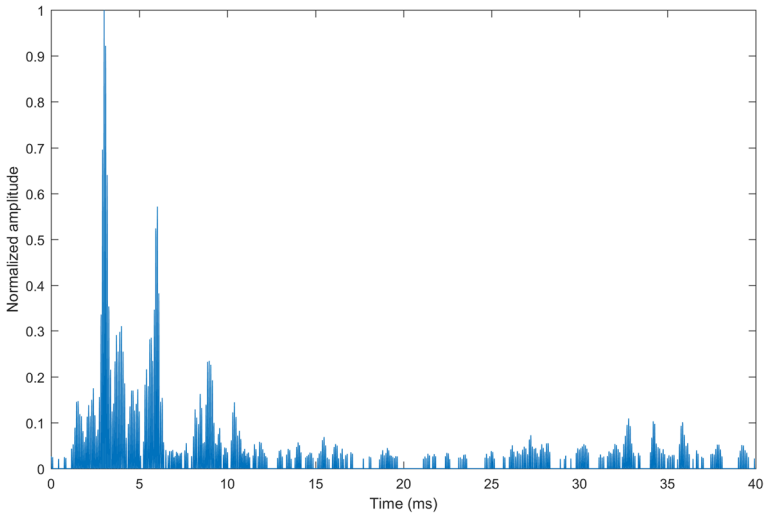

Fig. 5 Channel impulse response measured in the Qingjiang River

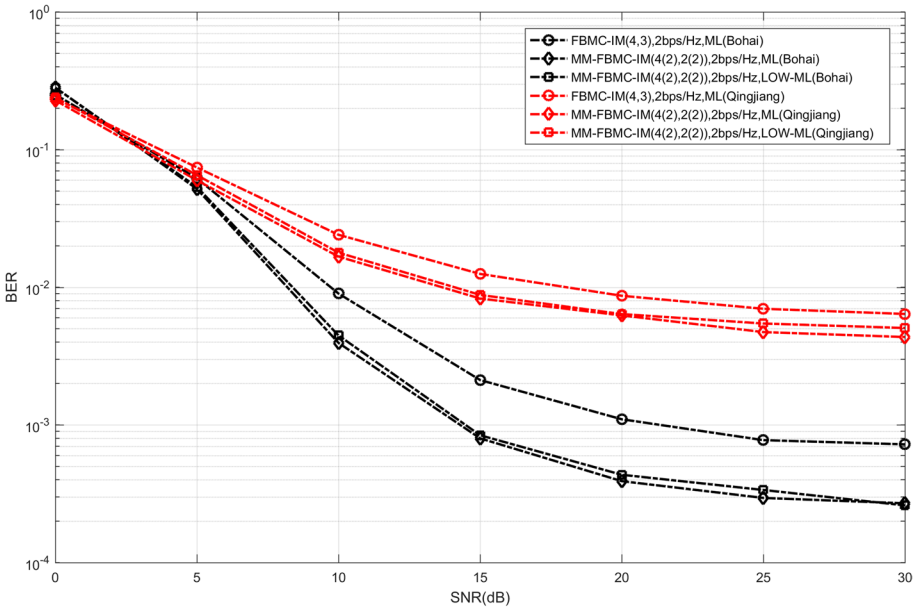

Fig. 6 Comparison of Algorithm Performance Across Different Underwater Acoustic Channels

The simulation parameters are shown in Table 2.

As shown in Fig. 4, our experimental data will be compared based on the measured underwater acoustic channel. The channel impulse response measured at 5 km in the Bohai Sea. The experimental site has a sea depth of about 50 m, with the transmitting transducer at approximately 15 m, and the receiving hydrophone at about 15 m deep. During the experiment, both the transmitting and receiving ships were on smooth-wavelet state. Figure 5 shows the measured channel impulse response of the Qingjiang River at a certain moment, which has been normalized. It can be observed that, compared to the Bohai Sea channel, the multipath effect in the Qingjiang channel is more severe. The

experiment was conducted at a water depth of approximately 100 m, with the transmitting transducer suspended at a depth of about 30 m and the receiving hydrophone suspended at a depth of about 10 m. The distance between the two was approximately 1.5 km, and both the transmitting and receiving vessels were in a state of free drifting. The challenges of deploying in underwater environments include channel complexity, system implementation difficulty, energy consumption, transmission distance limitations, and environmental noise interference. These challenges can be mitigated through adaptive technologies, optimized algorithms, and energy-saving strategies.

In Fig. 6, we present comparative experimental results of different algorithms across various underwater acoustic channels. From the figure, we can observe that MM-FBMC-IM exhibits certain advantages over traditional FBMC-IM, regardless of whether it is in the Bohai Sea channel or the Qingjiang River channel, even in a channel as multipath-rich as the Qingjiang River. It is also noteworthy that the proposed low-complexity ML detection algorithm shows nearly identical BER performance compared to the traditional ML detection algorithm, making this low-complexity algorithm feasible for practical systems. Subsequent experiments will be conducted in the Bohai Sea channel.

As shown in Fig. 7, the graph displays the different BER performances of traditional FBMC, FBMC-IM (4,3), QPSK and MM-FBMC-IM ($n = 4, M = 2$).FBMC-IM (4,3) indicates the selection of 3 out of 4 subcarriers for transmission; similar notations follow this convention. It can be seen that within the simulation setup, all maintain a spectral efficiency of 2bps/Hz. Furthermore, around a signal-to-noise ratio (SNR) of 12dB, FBMC-IM (4,3) begins to outperform the traditional FBMC system. Although the differences become minimal towards the end, their advantages still manifest. Looking at MM-FBMC-IM ($n = 4, M = 2$), it is observed that, with four modes and under such multiple mode conditions, the error rate of the index bits decreases very rapidly. This

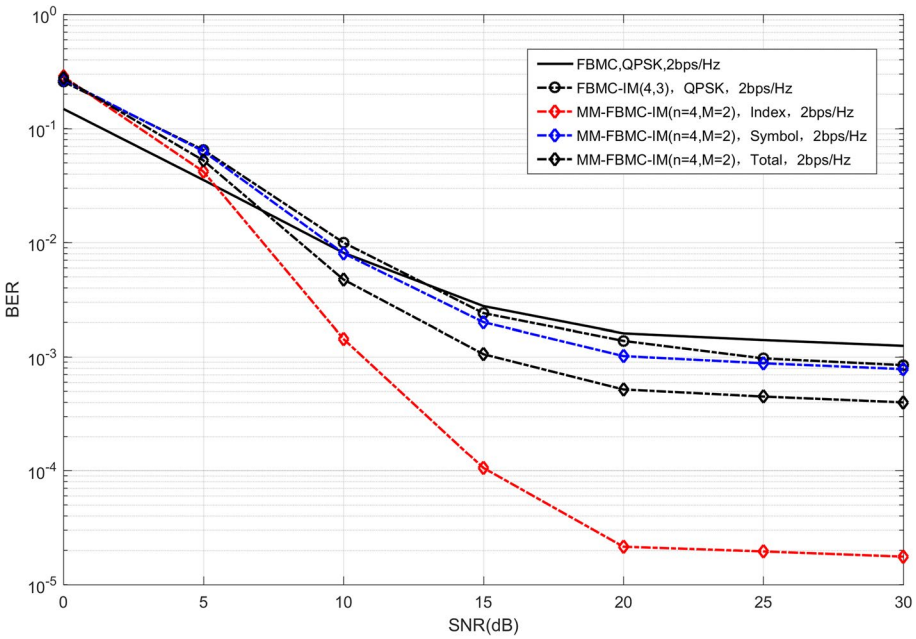

Fig. 7 BER curves of multiple mode with same order and different systems at a spectral efficiency of 2bps/Hz

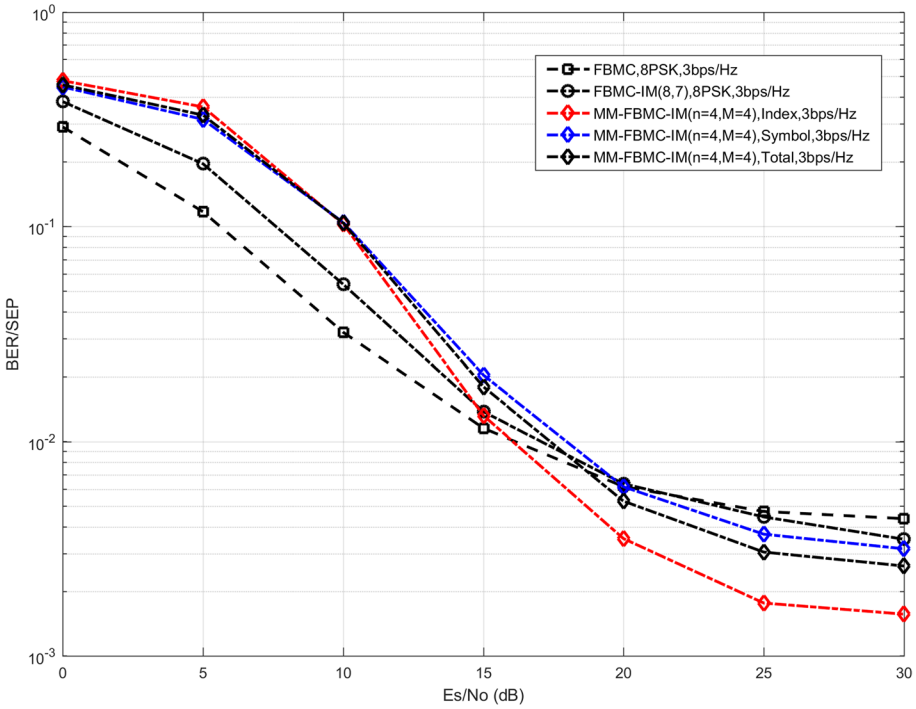

Fig. 8 BER Curves of multiple mode with same order and different systems at a spectral efficiency of 3bps/Hz

means that even with a higher bit load, the system can achieve a faster reduction in the error rate, especially at high SNR levels, where the benefits are even more pronounced.

In a similar comparison, when we increase the spectral efficiency to 3bps/Hz, we analyze the performance among traditional FBMC, FBMC-IM (8,7), and MM-FBMC-IM ($n = 4, M = 4$). As shown in Fig. 8, we can observe that the error rate of the index bits starts to decrease faster than the symbol error rate when the SNR reaches 10dB. Additionally, it's evident that at 3bps/Hz, the advantages brought by indexing still exist. Firstly, it's noticeable that the FBMC system, which selects 7 out of 8 subcarriers (FBMC (8, 7)), achieves a lower error rate than the traditional FBMC when the SNR reaches 20dB. Furthermore, the multiple mode indexing MM-FBMC-IM system exhibits better performance than the first two systems already at an SNR of 18dB.

Figure 9 depicts traditional FBMC with QPSK and 8PSK, FBMC-IM (8,5), and MM-FBMC-IM (4(2),2(2)). In this comparison, both FBMC-IM (8,5) and MM-FBMC-IM (4(2),2(2)) achieve a spectral efficiency of 2.5bps/Hz. In contrast, traditional FBMC using QPSK operates at a spectral efficiency of 2bps/Hz, while traditional FBMC with 8PSK reaches 3bps/Hz. We can observe that FBMC-IM (8,5) is positioned between traditional FBMC with QPSK and 8PSK. This is understandable, as different rates lead to varying error rates, with higher rates typically resulting in higher error rates. This positions the performance of FBMC-IM (8,5) in between those of the traditional FBMC implementations. However, MM-FBMC-IM (4(2),2(2)), with a rate of 2.5bps/Hz, shows performance at high SNR that can match or even surpass that of traditional FBMC at 2bps/Hz. At high SNR levels, the bits modulated through the indexing of multiple mode constellations are less prone to errors. This enhanced reliability allows the system's

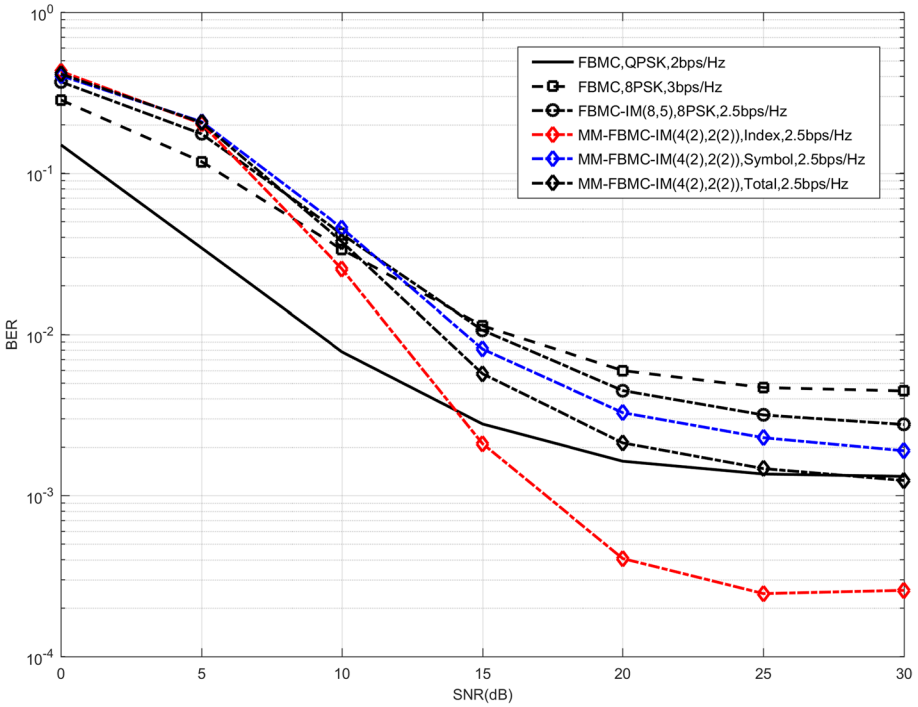

Fig. 9 BER curves of multiple mode with different orders and various systems

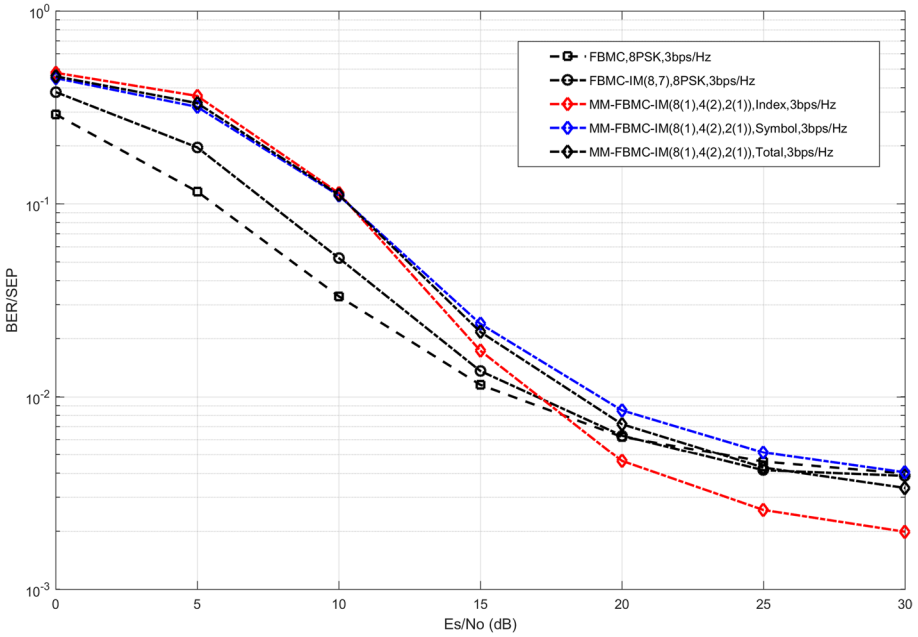

Fig. 10 BER curves of multiple mode with different orders and various systems at a spectral efficiency of 3bps/Hz

performance to compete with that of systems operating at lower rates, further highlighting the advantages of multi-modality.

As shown in Fig. 10, it showcases the different BER performances at a spectral efficiency of 3bps/Hz for the traditional FBMC with 8PSK, FBMC-IM (8,7), and MM-FBMC-IM (8(1),4(2),2(1)). It is observed that at this transmission rate, due to the reduced spacing between signal modes, the error rate performance of the systems deteriorates. The BER decline for FBMC-IM (8,7) aligns closely with that of traditional FBMC and 8PSK. However, MM-FBMC-IM (8(1),4(2),2(1)) still manages to secure a slight advantage at higher SNR levels.

5 Results and discussion

Based on the analysis of traditional FBMC and FBMC-IM, we emphasized their limitations in underwater acoustic channels, such as insufficient spectral efficiency and flexibility. By introducing multiple mode index modulation, the MM-FBMC-IM system effectively overcomes these challenges, particularly demonstrating significant advantages in spectral efficiency and system flexibility. Additionally, MM-FBMC-IM continues to outperform traditional methods across various underwater acoustic environments. However, as the complexity of the modes and the modulation order increases, the advantages of multiple mode indexing diminish. Therefore, future research needs to further optimize multiple mode indexing to maintain its advantages in complex FBMC systems.

Abbreviations

IM	Index modulation
OFDM	Orthogonal frequency division multiplexing
CP	Cyclic prefix
FBMC	Filter bank multicarrier
PAPR	Peak to average power ratio
MM-FBMC-IM	Multiple mode filter bank multicarrier with index modulation
BER	Bit error rate
ISI	Inter-symbol interference
ICI	Inter-carrier interference
OFDM-IM	Orthogonal frequency division multiplexing with index modulation
UWA	Underwater acoustic
IM-OFDM-SS	Index modulation orthogonal frequency division multiplexing spread spectrum
DM-OFDM	Dual mode orthogonal frequency division multiplexing
MM-OFDM-IM	Multiple mode orthogonal frequency division multiplexing with index modulation
CI	Coordinate interleaving
LCP	Linear constellation precoding
C-MM-OFDM-IM	Composite multiple-mode orthogonal frequency division multiplexing with index modulation
Y-FC	Y-shaped networks with fully connected layers
Y-BLSTM	Y-shaped networks with bidirectional long short-term memory units
OTFS	Orthogonal time frequency space
OTFS-IM	Orthogonal time frequency space index modulation
VBLAST	Vertical bell laboratories layered space-time
OTFS-DM-IM	Orthogonal time frequency space with dual-mode index modulation
FBMC-IM	Filter bank multicarrier with index modulation
CVNN	Complex valued neural networks
CNN	Convolutional neural networks
PSK	Phase shift keying
MIAD	Minimum intra-mode distance
MIRD	Minimum inter-mode distance
ML	Maximum likelihood
QPSK	Quadrature phase shift keying
QAM	Quadrature amplitude modulation

Acknowledgements

We sincerely thank all individuals and institutions who have provided support and assistance to this paper. This work was supported in part by the National Natural Science Foundation of China under Grant 52071164, the Postgraduate Research & Practice Innovation Program of Jiangsu Province under Grant KYCX24_4177, the Jiangsu Province Higher

Education Basic Science (Natural Science) Research Project under Grant No. 23KJB510003, and the National Defense Key Laboratory Fund for Underwater Acoustic Warfare Technology under Grant No. JCKY2024207CH09.

Author contributions
Z.Q.L. was primarily responsible for completing the writing of the paper. B.W. primarily handled the revisions of the paper and provided financial support. H.T.L. contributed significantly to data analysis and interpretation, as well as helping to refine the methodology and final discussion. T.F. provided suggestions for the paper's revision. Y.N.Z. provided technical support for the completion of the thesis and made partial revisions.

Funding
This work was supported in part by the National Natural Science Foundation of China under Grant 52071164, the Postgraduate Research & Practice Innovation Program of Jiangsu Province under Grant KYCX24_4177, the Jiangsu Province Higher Education Basic Science (Natural Science) Research Project under Grant No. 23KJB510003, and the National Defense Key Laboratory Fund for Underwater Acoustic Warfare Technology under Grant No. JCKY2024207CH09.

Availability of data and materials
Data availability is not applicable to this article.

Declarations

Competing interests
The authors declare that they have no competing interests.

Received: 11 June 2024 Accepted: 17 September 2024
Published online: 27 September 2024

References

1. K. Ramadan, M.I. Dessouky, S. Elagooz, M. Elkordy, F.E. Abd El-Samie, Equalization and carrier frequency offset compensation for underwater acoustic OFDM systems. Ann. Data Sci. **5**, 259 (2018)
2. Z.H. Gebeyehu, Impact of clipping noise on the sum rate of NOMA with PD-DCO-OFDM and conventional DCO-OFDM. Heliyon **6**(2), e03363 (2020). https://doi.org/10.1016/j.heliyon.2020.e03363
3. J. Choi, Coded OFDM-IM with transmit diversity. IEEE Trans. Commun. **65**, 3164 (2017)
4. J. Choi, Noncoherent OFDM-IM and its performance analysis. IEEE Trans. Wirel. Commun. **17**, 352 (2018)
5. M. Wen, X. Cheng, L. Yang, Y. Li, X. Cheng, F. Ji, Index modulated OFDM for underwater acoustic communications. IEEE Commun. Mag. **54**, 132 (2016)
6. Z.A.H. Qasem, H.A. Leftah, H. Sun, H. Esmaiel, Precoded IM-OFDM-SS for underwater acoustic communication. Wirel. Commun. Mob. Comput. **2022**, 1 (2022)
7. A. Fazeli, H.H. Nguyen, M. Hanif, Generalized OFDM-IM with noncoherent detection. IEEE Trans. Wirel. Commun. **19**, 4464 (2020)
8. T. Mao, Z. Wang, Q. Wang, S. Chen, L. Hanzo, Dual-mode index modulation aided OFDM. IEEE Access **5**, 50 (2017)
9. M. Wen, Q. Li, E. Basar, W. Zhang, Generalized multiple-mode OFDM with index modulation. IEEE Trans. Wirel. Commun. **17**, 6531 (2018)
10. Q. Li, M. Wen, E. Basar, H.V. Poor, B. Zheng, F. Chen, Diversity enhancing multiple-mode OFDM With index modulation. IEEE Trans. Commun. **66**, 3653 (2018)
11. J. Li, S. Dang, Y. Huang, P. Chen, X. Qi, M. Wen, H. Arslan, Composite multiple-mode orthogonal frequency division multiplexing with index modulation. IEEE Trans. Wirel. Commun. **22**, 3748 (2023)
12. Y. Zhu, B. Wang, J. Li, Y. Zhang, F. Xie, Y-shaped net-based signal detection for OFDM-IM systems. IEEE Commun. Lett. **26**, 2661 (2022)
13. S. Li, L. Xiao, X. Zhang, L. Li, T. Jiang, Spatial multiplexing aided OTFS with index modulation. IEEE Trans. Veh. Technol. **72**, 8192 (2023)
14. H. Zhao, D. He, Z. Kang, H. Wang, Orthogonal time frequency space (OTFS) with dual-mode index modulation. IEEE Wirel. Commun. Lett. **10**, 991 (2021)
15. X. Guo, B. Wang, Y. Zhu, Z. Fang, Z. Han, Hamming distance optimized underwater acoustic OTFS-IM systems. Entropy **25**, 972 (2023)
16. P. Kotipalli, A.S.M. Mohanraju, P. Vardhanapu, Frame boundary detection and deep learning-based doppler shift estimation for FBMC/OQAM communication system in underwater acoustic channels. IEEE Access **10**, 17590–17608 (2022). https://doi.org/10.1109/ACCESS.2022.3148410
17. X. Lu, Y. Jiang, Y. Wei, X. Tu, F. Qu, A Lattice-reduction-aided sphere decoder for underwater acoustic FBMC/OQAM communications. IEEE Wirel. Commun. Lett. **12**(3), 466–470 (2023). https://doi.org/10.1109/LWC.2022.3230857
18. G. Qiao, X. Liu, L. Ma, S. Mazhar, Y. Zhao, Residual doppler effect analysis of the FBMC/OQAM communication system in underwater acoustic channel. IEEE Commun. Lett. **25**, 3090 (2021)
19. J. Chu, M. Gao, X. Liu, M. Bi, H. Huang, G. Shen, Channel estimation based on complex-valued neural networks in IM/DD FBMC/OQAM transmission system. J. Light. Technol. **40**, 1055 (2022)
20. Y. Zhu, B. Wang, Y. Zhang, J. Li, C. Wu, convolutional neural network based filter bank multicarrier system for underwater acoustic communications. Appl. Acoust. **177**, 107920 (2021)
21. Z. Iqbal, F. Ji, J. Li, M. Wen, X. Qi, Multiple-input multiple-output multiple-mode OFDM with index modulation. IEEE Trans. Veh. Technol. **71**(12), 13441–13446 (2022). https://doi.org/10.1109/TVT.2022.3200977

22. W. Jin, M. Wang, G. Yang, Z. Chen, Energy-efficient and fading-resistant multi-mode OFDM-IM with high dimensional mapping. IEEE Trans. Wireless Commun. **22**(8), 5005–5017 (2023). https://doi.org/10.1109/TWC.2022.3230461
23. Y. Zhu, H. Huang, Z. Pu, B. Wang and Y. Li, Filter bank multicarrier communication with real part and imaginary part index modulation. IEEE Open J Commun Soc. https://doi.org/10.1109/OJCOMS.2024.3459955.
24. Y. Bian, X. Cheng, M. Wen, L. Yang, H.V. Poor, B. Jiao, Differential spatial modulation. IEEE Trans. Veh. Technol. (2014). https://doi.org/10.1109/TVT.2014.2348791

Publisher's Note